http://hdl.handle.net/2440/43095

Accurate and precise optical testing with a differential Hartmann wavefront sensor

Thu-Lan Kelly, Peter J. Veitch, Aidan F. Brooks, and Jesper Munch

A novel differential Hartmann sensor is described. It can be used to determine the characteristics of an optic accurately, precisely, and simply without detailed knowledge of the wavefront used to illuminate the optical system or of the geometry of the measurement system. We demonstrate the application of this sensor to both zonal and modal optical testing of lenses. We also describe a dual-camera implementation of the sensor that would enable high-speed optical testing.   © 2007 Optical Society of America

OCIS codes: 010.7350, 220.4840, 120.4640.

1. Introduction

The optical characteristics of systems that transmit or reflect light can be determined using a variety of techniques, including Hartmann[1–7] (H) and Shack–Hartmann[8–10] (S-H) wavefront sensors. S-H sensors, for example, are widely used to measure and control the effect of atmospheric turbulence in astronomical adaptive optics, as they are compatible with low light intensities and can operate at sampling rates of several kHz.[8,11] In many other applications, however, more light is available for the measurement, and the measurement time is less important. Thus a wavefront sensor that provides greater precision and accuracy, such as a Hartmann sensor, can be used.[5,12]

In H sensors, the centroids of the spots on the CCD camera and thus the transverse aberration produced by the optical system can be determined more precisely than in S-H sensors.[5] Furthermore, they are less sensitive to spatial variations in pixel responsivity and defective pixels and are obviously unaffected by defects in the micro-lens array.[10] The larger distance between the wavefront sampling element and the CCD, compared to that in a S-H sensor, further improves the precision with which the local slope of

the wavefront can be determined. These significant improvements in precision can compensate for the reduced spatial resolution of the H sensor to yield an improved measurement of the wavefront and of the characteristics of the optical system. Accurate determination of the characteristics, however, usually requires detailed knowledge of the incident reference wavefront and of the location of some of the cardinal planes.[6]

In this paper, we describe a differential Hartmann wavefront sensor that provides accurate, precise, and simple measurements of the characteristics of an optical system. This is achieved by combining transverse aberrations measured in two planes that are separated by an accurately and a precisely known distance. An alternative differential H sensor, in which a converging lens was placed in the back focal plane of the optical system and the transverse aberrations were measured in two planes equally spaced about that plane, was proposed by Roddier[2] as a means of doubling the sensitivity of the sensor. It did not consider the accuracy of the sensor, however.

We demonstrate the application of the differential Hartmann sensor to zonal and modal analyses of lenses, showing that the spherical power is reproducible to 0.1% for measurements spread over 1 week. The accuracy is demonstrated by comparing the measured power of a set of reference ophthalmic lenses with the nominal values. The modal analysis is performed using a dual-camera system that could enable high-speed measurement of the optical characteristics.

2. Differential Hartmann Sensor

The layout of the differential Hartmann sensor is shown schematically in Fig. 1. We will assume here that a transmissive optic is being characterized. The
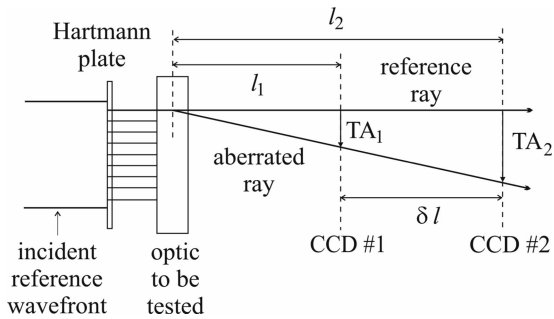
Fig. 1. Schematic layout of the differential Hartmann testing system. Only one of the rays produced by the Hartmann plate is traced through the optical system. When the unknown optic is placed in the path of the Hartmann ray, the ray is deflected to produce the "aberrated ray." A possible deflection is shown. The CCD camera is positioned at the locations denoted CCD 1 and CCD 2, to yield two transverse aberrations.

extension of the technique to reflective optics is straightforward.

As in the prototypic Hartmann optical testing system,[1,3–6] an opaque plate containing an array of holes, usually referred to as the Hartmann plate, is illuminated by a reference wavefront, thereby generating a set of Hartmann rays. The transverse position of these rays at a distant plane is recorded using a CCD camera. The optic is then inserted between the Hartmann plate and the CCD, and the "aberrated" transverse positions are recorded.

The wavefront aberration introduced by the optic, W, can be written as a linear combination of m modes: $W = \sum_{i=0}^{m-1} \alpha_i \Psi_i(x, y)$, where (x, y) denotes the coordinates at the optic. The transverse aberrations can thus be written[13]:

$$\mathrm{TA}_x = -l\,\frac{\partial W}{\partial x} = \sum_{i=0}^{m-1} a_i X_i, \qquad \mathrm{TA}_y = -l\,\frac{\partial W}{\partial y} = \sum_{i=0}^{m-1} a_i Y_i,$$
(2)

where

$$X_i = \frac{\partial \Psi_i}{\partial x}, \qquad Y_i = \frac{\partial \Psi_i}{\partial y}, \qquad a_i = -\alpha_i l,$$

and l is the lever-arm distance between the optic and the CCD.

The coefficients a_i can be determined by defining

$$\chi^2 = \sum_{j=1}^{N} \left\{ \left[\mathrm{TA}_{x_j} - \sum_{i=0}^{m-1} a_i X_i(x_j, y_j) \right]^2 \right.$$
$$\left. + \left[\mathrm{TA}_{y_j} - \sum_{i=0}^{m-1} a_i Y_i(x_j, y_j) \right]^2 \right\},$$
(3)

where N is the number of Hartmann rays, and solving $\partial \chi^2/\partial a_i = 0$. The resulting equations can be written conveniently as a matrix equation:

$$Ma = b,$$
(4)

where

$$M = X^T X + Y^T Y,$$

$$X = \begin{bmatrix} X_0(x_1, y_1) & \cdots & X_{m-1}(x_1, y_1) \\ \cdots & \cdots & \cdots \\ X_0(x_N, y_N) & \cdots & X_{m-1}(x_N, y_N) \end{bmatrix},$$

$$Y = \begin{bmatrix} Y_0(x_1, y_1) & \cdots & Y_{m-1}(x_1, y_1) \\ \cdots & \cdots & \cdots \\ Y_0(x_N, y_N) & \cdots & Y_{m-1}(x_N, y_N) \end{bmatrix},$$

$$a = \begin{bmatrix} a_0 \\ \cdots \\ a_{m-1} \end{bmatrix},$$

$$b = X^T b_x + Y^T b_y,$$

$$b_x = \begin{bmatrix} \mathrm{TA}_{x_1} \\ \cdots \\ \mathrm{TA}_{x_N} \end{bmatrix}, \qquad b_y = \begin{bmatrix} \mathrm{TA}_{y_1} \\ \cdots \\ \mathrm{TA}_{y_N} \end{bmatrix}.$$

The coefficients a_i are then calculated using $a = M^{-1}b$, where M^{-1} is usually determined using singular value decomposition (SVD).[14]

In a conventional Hartmann sensor, it is assumed that the lever-arm distance l is well defined, and thus the modal coefficients α_i can be calculated using Eq. (2). In systems that use a collimated reference wavefront, this assumption requires that the locations of the second principal plane of the optic and the active surface of the detector are known accurately.[6] While the second requirement may be reasonable, the first will limit the applicability and accuracy of this technique. This calculation would be even more problematic if the reference wavefront was not collimated, as the plane from which l should be measured cannot a priori be well defined. Furthermore, the coordinates of the Hartmann rays at the optic must be estimated from the layout of the system (see Ref. 7 for example), which may further reduce the accuracy and precision.

The reliance on the accuracy of l can be eliminated by using an additional set of transverse aberrations, measured after moving the CCD to a second location CCD 2, separated from the first recording location, CCD 1, by a precisely and accurately known distance δl. The modal coefficients α_i are then calculated using

$$\alpha_i = (a_{i1} - a_{i2})/\delta l,$$
(5)

where a_{i1} and a_{i2} are the coefficients in the first and second planes. A detailed example of this analysis using Seidel aberrations is given in Appendix A. This procedure can be extended to multiple measurement planes by plotting a_{ik} as a function of δl_k and determining the slope of the line of best fit.

Using a collimated reference wavefront simplifies the analysis, as the Hartmann ray coordinates at the optic can be obtained directly from the centroids of the reference spots at the CCD. The relative separation of the reference spots at the two CCD locations
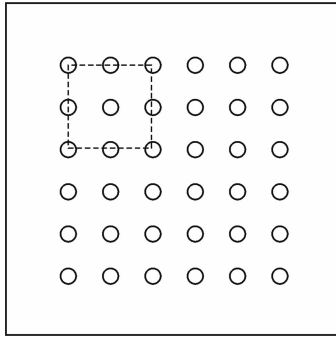
Fig. 2. Schematic of a Hartmann plate with a 6 × 6 square array of holes. Dividing the holes into 3 × 3 subsets, one of which is shown, and using a spot-centered analysis would allow the optical parameters to be determined at 16 locations. Including non-spot-centered subsets would allow the parameters to be calculated at other locations.

can be used to determine whether the reference wavefront is collimated.

The differential Hartmann sensor can be used for both modal and zonal analysis of the optic. For zonal analysis, the Hartmann rays are divided into sets of adjacent rays. For example, spots produced by a square-array Hartmann plate could be divided into subsets of nine spots, and the analysis might be centered on the central spot ("spot-centered"), as shown in Fig. 2, or at a point between the spots. Other hole patterns, such as hexagonal-close-packed (hcp), which would improve the spatial resolution, could also be used. However, as discussed further in Subsection 3.A, hcp arrays are not suitable for distinguishing between defocus and spherical aberration.

3. Demonstration of the Differential Hartmann Sensor

The differential Hartmann sensor can be implemented using a variety of techniques: the camera can be moved between the measurement planes, or a transparent optical flat could be used to change the optical length of the lever arm, or a beam splitter and two cameras could be used to measure simultaneously the transverse aberrations.

In this section we describe two proof-of-principle tests that use the moving-camera and dual-camera implementations and demonstrate the sensitivity and accuracy of the differential Hartmann sensor. First, we describe the zonal analysis of a high-quality microscope objective lens using a single movable camera in which δl was set using a solid spacer block. We then describe the modal analysis of a series of ophthalmic reference lenses using a dual-camera system. For both tests, spot centroids were determined using image processing to detect the spots and iterative fractional pixel interpolation to determine the centroids, as will be detailed in another paper.[15]

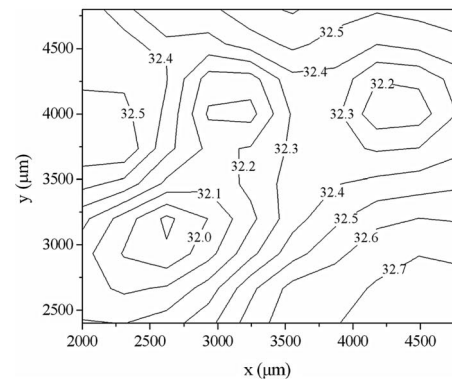### A. Zonal Spherical Power Map of a Microscope Objective Lens

A Hartmann plate consisting of a hexagonally close-packed array of 0.3 mm diameter holes separated by

0.6 mm was used for this measurement. The camera was mounted on an optical rail, and the distance δl was set using a solid spacer block that had parallel faces, the length of which was measured using Vernier calipers. Due to the short focal length, $f \approx 30$ mm, of the objective lens, the second set of transverse aberrations was recorded with the CCD located beyond the back focal plane of the lens. A combination of prismatic, defocus, and, astigmatic aberrations was used to describe the optic. The analysis was performed using seven-element spot-centered subsets, yielding defocus values at locations as shown in Fig. 3(a), which are within the central 50% of the lens aperture. The defocus at each position was reproducible to ± 0.03 diopter, corresponding to $\Delta f/f = 1 \times 10^{-3}$ or $\Delta f = 30$ μm, for measurements spread over 1 week. A contour map, shown in Fig. 3(b), was generated using these defocus values. Note that the contour interval in this map is 3 times larger than the reproducibility of the values used to construct the map.

The "spot-centered" analysis was extended to include spherical aberration and coma but it produced
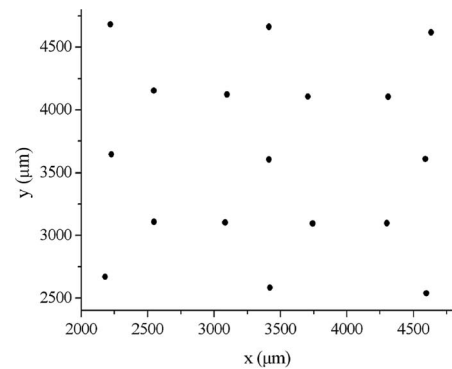
(a)

(b)

Fig. 3. (a) Plot of the 17 locations at which the zonal spherical power of the microscope objective lens was calculated. The central location is near the optical axis of the lens. (b) A contour map of the spherical power of a microscope objective lens. The zonal measurements of spherical power were transformed into a 10 × 10 regular grid with smoothness parameter = 0.6 using the correlation (Kriging) method in the Microcal Origin package. The 0.1 diopter contour interval is 3 times larger than the reproducibility of the measurements used to generate the plot.

large variations in the spherical power and much larger residuals, due to the difficulty in distinguishing between defocus and spherical aberration using a set of spots that have essentially the same radial distance from the central spot. This ill-conditioning was removed when using a non-spot-centered analysis. Alternatively, a square array or an array optimized to differentiate between these two particular aberrations would also prevent the ill-conditioning but may have lower spatial resolution. This reveals the opportunity to optimize the array for a particular measurement. If, for example, power and spherical aberration were to be differentiated, and since they have different dependences on radius, a purpose-designed Hartmann plate with a spiral array of holes could yield improved results.

B. Dual-Camera Modal Analysis of Ophthalmic Reference Lenses

A schematic of the measurement system used to characterize the ophthalmic lenses is shown in Fig. 4. The light source for these measurements was a fiber-coupled superluminescent LED (SLED) emitting 50 μW at 820 nm. The Hartmann plate initially consisted of a square array of 1.0 mm diameter holes separated by 3.0 mm. A pellicle beam splitter was used to divide the Hartmann rays and to prevent multiple reflections. The cameras used 6.66 mm × 5.32 mm complementary metal-oxide semiconductor (CMOS) sensors and 8-bit digitization but had 1–2 bits of noise. The difference between the distances to the two sensors, $\delta l_{\text{sensors}}$, was determined by using an optical wedge to introduce a known prismatic aberration.

Since the Hartmann array was larger than the CMOS sensor, and indeed the CCD sensor used previously, a flat-field projector lens was used to reduce the lateral extent of the Hartmann spot pattern. However, as the sensors were necessarily at different distances from this lens, the reduction factors, R_1 and R_2 (R_1, $R_2 < 1$), were also different. Typical Hartmann spot patterns are shown in Fig. 5.

The reduction factors were measured using a Hartmann plate located at the position of the unknown optic, illuminating it with a collimated reference
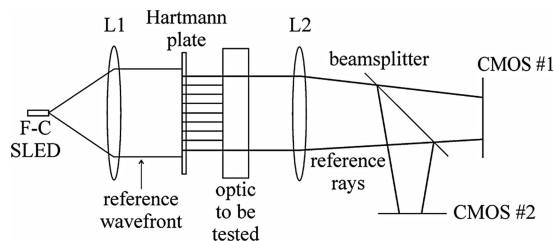

Fig. 4. Schematic layout of the differential Hartmann sensor used for the modal analysis of the reference lenses. A beam splitter and two CMOS sensors were used to implement the differential measurement. A fiber-coupled (F-C) SLED light source was used to prevent unwanted interference fringes. The demagnifying lens, L2, reduces the size of the Hartmann spot pattern to that of the CMOS sensors.
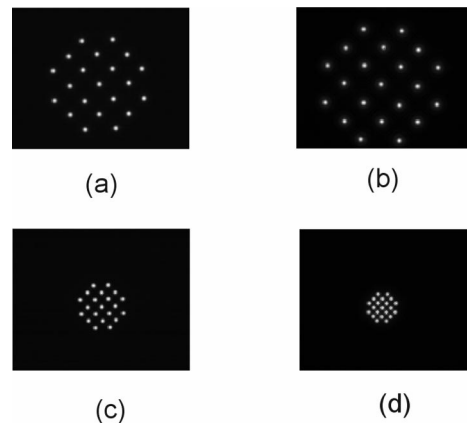

Fig. 5. Images of Hartmann spot patterns for a 4 diopter lens with $\delta l_{\text{sensors}} = 9.20$ mm, $R_1 = 0.360$, and $R_2 = 0.450$: (a), (b) reference spots at planes 1 and 2; (c), (d) "aberrated" spot at planes 1 and 2, located after the focal plane of the 4 diopter lens.

wave and comparing the spot positions with those measured without the reduction lens. The measured transverse aberrations, TA_1 and TA_2, and $\delta l_{\text{sensors}}$, were then transformed using $TA_1' = TA_1/R_1$, $TA_2' = TA_2/R_2$ and $\delta l' = \delta l_{\text{sensors}}/R_1 R_2$, and these values were used for the analysis.

Alternatively, the analysis could have been performed using the measured transverse aberrations and the differential arm length calibrated with the reduction lens in place. However, this would require either a prior measurement of the Hartmann beam coordinates at the optic or that these coordinates were calculated using the reference spot positions and the measured reduction factors. Additionally, the maximum wedge angle that could be used for the length calibration would be reduced. Using a large CMOS or CCD sensor would remove the need for the reduction lens and thus simplify the analysis significantly.

The transverse aberrations were analyzed for prism (P), spherical (S), and cylindrical (C) powers, coma (B), and spherical aberration (A). Initially, a 3×3 set of holes was used for the analysis; however, the SVD indicated that the M matrix was singular, due to the very small spherical aberration expected for these lenses. Increasing the number of holes, typically to 13–21 holes, removed the ill-conditioning but could lead to including barrel distortion from the reduction lens.

The measured P, S, and C are listed in Table 1. They are similar to those determined by analyzing the 3×3 sets for P, S, and C only, and show good agreement with the nominal values and a reproducibility of ~1%. The tolerance on the nominal power of the reference lenses is unknown but is assumed to be less than the ±0.06 diopter manufacturing tolerance on single-vision ophthalmic lenses.[6]

The nonzero P values in Table 1 may indicate that the Hartmann plate was not accurately aligned with the center of the lens. The nonzero C values may indicate an angular misalignment of the ref-

Nominal			Measured		
S	C	P	S	C	P
1.5	0.0	0.0	1.49 ± 0.02	0.001 ± 0.01	0.0002 ± 0.0001
2.0	0.0	0.0	1.98 ± 0.01	-0.09 ± 0.01	0.0002
2.25	0.0	0.0	2.23 ± 0.02	-0.15 ± 0.03	0.0003
3.0	0.0	0.0	3.02 ± 0.04	-0.01 ± 0.01	<0.0001
3.5	0.0	0.0	3.52 ± 0.01	-0.01 ± 0.002	<0.0001
4.0	0.0	0.0	3.94 ± 0.08	0.03 ± 0.02	-0.001 ± 0.0003
4.5	0.0	0.0	4.54 ± 0.02	0.01 ± 0.03	0.0002 ± 0.0006
5.0	0.0	0.0	5.07 ± 0.02	0.04 ± 0.03	<0.0001

[a]S and C are in diopters.

erence wavefront and the optical axis of the lens. Coma (B) and spherical aberration (A) were also expected to be small for these lenses. Coma values were generally nonzero, which is consistent with the nonzero C values, and were reproducible. The spherical aberration coefficients, by contrast, were not reproducible, even though the M matrix was not ill-conditioned. The difference in reproducibility between coma and spherical aberration is probably because spherical aberration dominates over other third-order aberrations for large apertures, as $\text{TA}_{\text{spherical aberration}} \propto \text{aperture}^3$ while $\text{TA}_{\text{coma}} \propto \text{aperture}^2$, and thus it is more sensitive to readout noise. This problem could be fixed by using cameras with larger dynamic range (more digitization bits and/or less noise). Additionally, a Hartmann plate with an optimized hole pattern that enabled the transverse aberration to be measured at a larger number of radii might improve the reproducibility of A, as discussed above.

4. Conclusion

We have described a differential Hartmann wavefront sensor that can simply, precisely, and accurately determine the properties of an optical system without the need for accurate knowledge of the location of the cardinal planes of the optical system, of the geometry of the measurement system, or of the reference wavefront. We have demonstrated that the sensor has excellent reproducibility over extended time frames, has good accuracy, and can be used for both modal and zonal analysis. We have also described a dual-camera implementation of the differential sensor that can be used for high-speed characterization and would be suitable for industrial lens quality assurance.

averaging can enable measurement of wavefront changes with a reproducibility of about $\lambda/4000$ over second time scales and about $\lambda/250$ over 24 hours.[12] Using these optimized sensors in the differential layout described here would allow ultraprecise and accurate characterization of optical systems.

Appendix A: Example of Modal Analysis for Seidel Aberrations

The wavefront might be described using Seidel aberrations, giving up to third order[3]

$$
\begin{aligned}
W = {} & P(x \cos \alpha + y \sin \alpha) + 0.5S(x^2 + y^2) \\
& + 0.5C(x \sin \phi - y \cos \phi)^2 + B(x \cos \beta + y \sin \beta) \\
& \times (x^2 + y^2) + A(x^2 + y^2)^2,
\end{aligned} \tag{A1}
$$

where P is the prism, α is the orientation of the prism, S is the defocus or spherical power, C is the astigmatism or cylindrical power, ϕ is the orientation of the cylinder, B is the coma, β is the orientation of the coma, A is the spherical aberration, and x and y are the coordinates of the Hartmann ray at the optic.

Using Eq. (2), the expected transverse aberrations can be written

$$
\begin{aligned}
\text{TA}_x = {} & a_0 + a_1 x + a_2 y + 2a_3 xy + 3a_4 x^2 + a_4 y^2 + a_5 x^3 \\
& + a_5 xy^2,
\end{aligned} \tag{A2a}
$$

$$
\begin{aligned}
\text{TA}_y = {} & a_6 + a_2 x + a_7 y + 2a_4 xy + a_3 x^2 + 3a_3 y^2 + a_5 y^3 \\
& + a_5 x^2 y,
\end{aligned} \tag{A2b}
$$

where the coefficients are given by

$$
\begin{aligned}
&a_0 = -lP \cos \alpha, && a_1 = -l(S + C \sin^2 \phi), \\
&a_2 = l(C \sin \phi \cos \phi), && a_3 = -lB \sin \beta, \\
&a_4 = -lB \cos \beta, && a_5 = -l4A, \\
&a_6 = -lP \sin \alpha, && a_7 = -l(S + C \cos^2 \phi).
\end{aligned} \tag{A2c}
$$

The coefficients a_i can be determined by defining

$$
\begin{aligned}
\chi^2 = \sum_{j=1}^{N} \Big\{ & \left[\text{TA}_{x_j} - \left(a_0 + a_1 x_j + a_2 y_j + 2a_3 x_j y_j + 3a_4 x_j^2 + a_4 y_j^2 + a_5 x_j^3 + a_5 x_j y_j^2 \right) \right]^2 \\
& + \left[\text{TA}_{y_j} - \left(a_6 + a_2 x_j + a_7 y_j + 2a_4 x_j y_j + a_3 x_j^2 + 3a_3 y_j^2 + a_5 y_j^3 + a_5 x_j^2 y_j \right) \right]^2 \Big\},
\end{aligned} \tag{A3}
$$

Further optimization of the Hartmann wavefront sensor using 12-bit dynamic range CCD cameras and

where TA_x and TA_y are the measured transverse aberrations in the x and y directions, and by solving the

set of equations arising from $\partial \chi^2/\partial a_i = 0$. Note that since the reference wavefront is collimated, the (relative) positions of the Hartmann rays, (x, y), at the input aperture of the optic are the same as their reference positions at the CCD. Comparison of Eq. (A3) with Eq. (3) yields

$$
\begin{array}{ll}
X_0 = 1, & Y = 0, \\
X_1 = x, & Y_1 = 0, \\
X_2 = y, & Y_2 = x, \\
X_3 = 2xy, & Y_3 = x^2 + 3y^2, \\
X_4 = 3x^2 + y^2, & Y_4 = 2xy, \\
X_5 = x^3 + xy^2, & Y_5 = y^3 + x^2y, \\
X_6 = 0, & Y_6 = 1, \\
X_7 = 0, & Y_7 = y.
\end{array}
\tag{A4}
$$

The matrix M is formed as described in Eq. (4) and inverted to yield the coefficients a_i, and the orientation angles and characteristic-length products are calculated using

$$
\tan \alpha = a_6/a_0, \tag{A5a}
$$

$$
\tan 2\phi = 2a_2/(a_1 - a_7), \tag{A5b}
$$

$$
\tan \beta = a_3/a_4, \tag{A5c}
$$

$$
Pl = \left(a_0{}^2 + a_6{}^2\right)^{1/2}, \tag{A5d}
$$

$$
Cl = \begin{cases} (a_1 - a_7)/\cos 2\phi, & \cos 2\phi \neq 0 \\ a_2/\cos \phi \sin \phi, & \cos 2\phi = 0 \end{cases}, \tag{A5e}
$$

$$
Sl = -(a_1 + a_7 + Cl)/2, \tag{A5f}
$$

$$
Bl = \left(a_3{}^2 + a_4{}^2\right)^{1/2}, \tag{A5g}
$$

$$
Al = -a_5/4. \tag{A5h}
$$

By convention, ϕ is assumed to be between 0 and π.

Since the distance l is not known accurately, the measurements are repeated in a second plane and the parameters described in Eqs. (A5a)–(A5h) recalculated. Then, the optical characteristics are calculated using

$$
P = (Pl_2 - Pl_1)/\delta l, \tag{A6a}
$$

$$
C = (Cl_2 - Cl_1)/\delta l, \tag{A6b}
$$

$$
S = (Sl_2 - Sl_1)/\delta l, \tag{A6c}
$$

$$
B = (Bl_2 - Bl_1)/\delta l, \tag{A6d}
$$

$$
A = (Al_2 - Al_1)/\delta l, \tag{A6e}
$$

where Pl_k is the characteristic-length product estimate in the kth plane, and similarly for the other quantities, obtained from Eqs. (A5d)–(A5h). The results of Eqs. (A5a)–(A5c) can be averaged to yield an improved value for the orientation angles.

References

1. I. Ghozeil, "Hartmann and other screen tests," in *Optical Shop Testing,* D. Malacara, ed. (Wiley, 1992), Chap. 10, pp. 367–396.
2. F. Roddier, "Variations on a Hartmann theme," Opt. Eng. **29,** 1239–1242 (1990).
3. D. Malacara and Z. Malacara, "Testing and centering of lenses by means of a Hartmann test with four holes," Opt. Eng. **31,** 1551–1555 (1992).
4. C. Castellini, F. Francini, and B. Tiribilli, "Hartmann test modification for measuring ophthalmic progressive lenses," Appl. Opt. **33,** 4120–4124 (1994).
5. V. Laude, S. Olivier, C. Dirson, and J.-P. Huignard, "Hartmann wave-front scanner," Opt. Lett. **24,** 1796–1798 (1999).
6. D. P. Salas-Peimbert, G. Trujillo-Schiaffino, J. A. González-Silva, and S. Almazán-Cuellar, "Simple Hartmann test data interpretation for ophthalmic lenses," Rev. Sci. Instrum. **77,** 043102 (2006).
7. M. Servin, F.J. Cuevas, D. Malacara, and J. L. Marroquin, "Direct ray aberration estimation in Hartmanngrams by use of a regularized phase-tracking system," Appl. Opt. **38,** 2862–2869 (1999).
8. R. K. Tyson, *Principles of Adaptive Optics* (Academic, 1991).
9. M. Abitol, A. Blum, A. Halimi, and E. Meimoun, "Apparatus for mapping optical elements," U.S. patent 5,825,476 (20 October 1998).
10. J. Pfund, N. Lindlein, and J. Schwider, "Dynamic range expansion of a Shack–Hartmann sensor by use of a modified unwrapping algorithm," Opt. Lett. **23,** 995–997 (1998).
11. M. A. van Dam, D. L. Mignant, and B. A. Macintosh, "Performance of the Keck Observatory adaptive optics system," Appl. Opt. **43,** 5458–5467 (2004).
12. A. F. Brooks, P. Veitch, and J. Munch, "Ultra-sensitive wave-front measurement using a Hartmann sensor," presented at the Australian Institute of Physics 17th National Congress, Brisbane, Australia, 3–7 December 2006.
13. W. H. Southwell, "Wave-front estimation from wave-front slope measurements," J. Opt. Soc. Am. **70,** 998–1006 (1980).
14. W. H. Press, S. A. Teukolsky, W. T. Vetterling, B. P. Flannery, in *Numerical Recipes in C,* 2nd ed. (Cambridge University, 1992), pp. 59–70.
15. T.-L. Kelly, A. F. Brooks, P. J. Veitch, and J. Munch, "Centroid estimation for Hartmann wavefront sensors," manuscript in preparation.